Crystallization Kinetics of Poly(L-lactide-*co*-*meso*-lactide)

JEFFREY J. KOLSTAD

Central Research, Cargill, Inc., Minneapolis, Minnesota 55440

SYNOPSIS

The crystallization kinetics of poly(L-lactide-*co*-*meso*-lactide) were determined over a range of 0% to 9% mesolactide. The kinetics were fit to the nonlinear Avrami equation and then to the Hoffman–Lauritzen equation modified for optical copolymers. The theory was found to fit the data well. The crystallization half-time was found to increase about 40% for every 1 wt % *meso*-lactide in the polymerization mixture. The change in crystallization rate is driven mainly by the reduction in melting point for the copolymers. The copolymer crystallization kinetics were also determined in the presence of talc, a nucleating agent for polylactide. The theory again fit the data well, using the same growth parameters and accounting for the talc only through the nucleation density term. © 1996 John Wiley & Sons, Inc.

INTRODUCTION

Polylactide is being developed as a biodegradable replacement for conventional thermoplastics. Although expensive, it has long been used as a copolymer in the medical field, providing resorbable sutures, implants, and controlled release of drugs. Recent development of a continuous process[1] has lowered the price of polylactide to the point where it is now competitive with other degradable polymers and potentially competitive with petroleum derived plastics.

Lactide exists in three stereoisomeric forms, L-lactide, D-lactide, and *meso*-lactide. It is prepared by depolymerization of low-molecular-weight poly(lactic acid) and the three isomers are formed nearly in proportion to statistical expectation. Denoting the weight fraction of L-lactic acid as S and the weight fraction of D-lactic acid as R, the expected weight fractions of the lactide isomers will be S^2 (L-lactide), $2RS$ (*meso*-lactide), and R^2 (D-lactide). For mixtures with low values of R, the crude lactide will contain a trace of D-lactide (1% at $R = 0.1$) with L-lactide (81% at $R = 0.1$) and mesolactide (18% at $R = 0.1$). Control of the lactic acid optical composition gives control of the lactide composition, which in turn offers control over many of the properties of the final polymer. Understanding the effect of copolymerization of *meso*-lactide with L-lactide on the crystallization kinetics is important in designing the best polymer composition for a given application.

The optical composition affects the rate of crystallization, the extent of crystallization, and the melting point. The impact on melting point is particularly significant because poly(L-lactide), which has an equilibrium melting point of about 207°C,[2-4] has a practical melting point of about 180°C when crystallized at temperatures of about 100°C. The minimum processing temperature of a polymer is typically about 20°C above the melting point, leading to a processing temperature for poly(L-lactide) of 200°C or higher. Introduction of *meso*-lactide can easily depress the melting point by 20 to 50°C, allowing processing at temperatures of about 150 to 180°C. There is a significant processing benefit to the lower temperatures, including lower rates of hydrolytic degradation, lower rates of oxidative degradation, lower rates of lactide vaporization/reformation, and better viscosity characteristics.

Previous studies have investigated the crystallization behavior of poly(L-lactide),[2-7] poly(L-lactide-*co*-D-lactide),[8] or the stereocomplex formation between poly(L-lactide) and poly(D-lactide).[9-12] Essentially no data on copolymers of L-lactide and mesolactide have been published. This is due to the practice of purifying lactide through recrystallization from a solvent, which precipitates the L- and D-lactides but leaves the mesolactide in solution with

Journal of Applied Polymer Science, Vol. 62, 1079–1091 (1996)
 CCC 0021-8995/96/071079-13

Table I Isothermal Crystallization Data

Temperature (°C)	*meso* (wt %)	3 min	5 min	7 min	9 min	16 min	$H_f(\infty)$	n
85	0	0.9	3.3	6.9	12.1	34.1	51	2.5
90	0	4.0	16.4	30.2	39.6	48.5	48	2.5
95	0	13.7	36.2	43.2	44.9	47.8	46	2.7
100	0	21.7	40.7	43.4	44.5	47.0	45	2.4
105	0	31.5	43.5	45.1	45.9	47.7	46	—
110	0	38.9	48.0	49.9	51.2	53.6	53	—
115	0	23.1	48.3	52.7	53.9	55.5	54	2.7
125	0	5.3	29.3	50.1	56.7	57.8	57	3.4
130	0	1.0	7.0	18.2	32.5	56.6	57	3.2
135	0	1.0	1.4	2.5	3.9	14.9	(57)	2.4
85	3	0.8	2.9	4.9	6.9	15.8	(46)	1.6
90	3	1.0	5.8	11.5	18.2	42.6	(46)	2.6
95	3	1.8	9.7	20.2	31.0	45.9	46	2.7
100	3	0.5	5.9	14.3	24.2	45.5	46	2.9
105	3	0.4	6.4	16.3	28.2	47.5	48	3.2
110	3	3.6	17.7	34.6	44.5	49.5	49	3.0
115	3	2.0	11.7	26.6	39.8	50.4	50	3.1
120	3	0.9	6.7	17.7	31.2	51.0	51	3.2
125	3	1.2	3.7	7.5	13.6	45.3	(51)	3.2
130	3	0.1	0.7	1.1	1.6	3.9	—	—
100	6	0.6	1.7	2.3	3.1	9.1	[44]	1.8
105	6	0.3	1.1	1.8	3.2	14.3	[44]	2.7
110	6	−0.4	−1.0	0.9	2.1	12.8	[44]	3.6
115	6	0.3	1.3	2.0	3.0	11.6	[44]	2.4

Values of J/g, PLA basis. $H_f(\infty)$ values in parentheses are estimated from adjacent temperature. Values in square brackets are from a separate annealing experiment. All other $H_f(\infty)$ values and n determined by nonlinear least-squares regression.

impurities from which it is difficult to recover.[13-14] Purification of crude lactide by distillation has now yielded mixed streams of L- and *meso*-lactide in commercial quantities. This is thought to be the first report on the crystallization behavior of poly(L-lactide-*co*-*meso*-lactide).

EXPERIMENTAL

Laboratory vial polymerizations were used to prepare the samples in this study, except for pilot plant samples used for the samples in Table IV and Figure 6. Previous work (unpublished) has shown that copolymers of L-lactide and *meso*-lactide prepared under the conditions of this study are essentially random, with only 14% relative reactivity difference in the monomers.

The vial polymerizations used, typically, L-lactide from Boehringer Ingelheim (*S*-grade), used as received, and *meso*-lactide from PURAC, used either as received or after vacuum distillation. The *meso*-lactide was found to contain up to 5% of D- and L-lactide, after the vacuum distillation. Vial polymerizations were performed by melting the lactide monomer in a round-bottom flask with a nitrogen purge and stirring. Catalyst, tin II bis(2-ethyl hexanoate), was then added as a 10 wt % solution in either tetrahydrofuran (THF) or toluene. Aliquots were then pipetted into silanized glass vials, capped, and placed into an oil bath at 180°C and polymerized for 4 h. The monomer-to-catalyst molar ratio was 5,000 : 1 for the samples in Table I and 10,000 : 1 for samples in Table II. After polymerization the vials were quenched in liquid nitrogen and broken to obtain the polymer plugs. Analysis by gel permeation chromatography (GPC) across a representative vial showed consistent molecular weight.

The pilot plant polymerizations were carried out in 2 CSTRs in series with nominal volumes of 1 gallon and 5 gallons. The catalyst was tin II bis(2-ethyl hexanoate), added neat to the monomer stream. The polymerization temperature was about 180 to 200°C. The polymer was removed from the reactor through a melt pump, passed through a die,

Table II Isothermal Crystallization Data, Set 2

Temperature (°C)	*meso* (wt %)	2 min	3 min	4 min	5 min	6 min	9 min	13 min	16 min	$H_f(\infty)$	n
90	0	−0.1	0.6	2.1	4.5	7.1	16.4	31.0	40.7	51	2.5
100	0	5.8	9.7	17.7	27.4	34.6	39.1	37.2	35.1	37	3.1
110	0	7.6	14.1	24.7	35.7	42.6	47.7	47.2	46.1	47	2.7
120	0	1.9	4.7	10.0	18.3	27.8	47.8	50.3	49.4	50	3.3
130	0	2.1	2.2	3.2	4.1	5.1	10.7	23.6	35.9	(50)	2.7
100	3	0.2	0.5	2.1	4.2	6.2	12.9	24.6	34.7	(47)	2.4
110	3	−0.7	−0.4	1.2	3.2	5.4	13.4	27.8	38.2	47	2.9
120	3	−0.6	0.3	1.8	3.5	5.2	11.5	24.4	35.7	(47)	2.8
100	6	−0.6	−0.3	0.7	1.5	2.2	2.6	3.2	3.6	—	—
110	6	−0.6	−0.2	0.8	1.4	1.7	2.5	3.8	5.5	—	—

Values in J/g, PLA basis. $H_f(\infty)$ values in parentheses are estimated from adjacent temperature. All other $H_f(\infty)$ values and n determined by nonlinear least-squares regression.

cooled as a strand in a water bath, and pelletized. The polymer was then dried and devolatilized, followed by repelletizing. The lactide was supplied by a lactide production pilot plant. After purification by distillation it consisted of approximately 91% L-lactide and 9% *meso*-lactide, for the samples in Table IV. Various levels of meso were used to obtain the samples in Figure 6.

Talc was added to the samples by compounding in a Brabender mixing head at 177°C for samples in Table V, using Ultratalc™ 609 from Pfizer. The samples were then pressed into films and devolatilized under high vacuum for 4 h at 120°C. The films were then sampled for the differential scanning calorimetry (DSC) tests. The samples in Table IV were compounded on a Leistritz twin screw extruder with talc addition through a K-tron feeder.

Crystallization and analysis were carried out using a Mettler Model 30 Differential Scanning Calorimeter, calibrated with an indium standard. Fifteen-minute isothermal runs were used to generate most of the data. For these runs, a sample was heated from 60°C to 200°C at 20°C/min, held 2 min for melt-out, quenched to the desired isothermal temperature (rate of about 200°C/min), held for 1 min (machine settling time), then held for an additional 15 min. The sample was then quenched to 60°C and heated to 200°C at 20°C/min to measure the crystallinity at t = 16 min (the 1-min settling time is essentially all at the isothermal temperature and has been added to the reported times). The isothermal heat-flow curve was integrated to various time points to determine the crystallinity as a function of time. The final melt-out was used to correct for any zero offset and was applied proportionally to the samples at intermediate times.

For the fastest crystallizing materials (Table V) the isothermal integration was inaccurate and the method was replaced by running isothermals of the desired time length, followed by quenching and a melt-out to determine the crystallinity for that period of time. Hold times of 30 s, 1 min, 2 min, and 3 min were used.

All runs were made in randomized order to avoid bias due to molecular weight degradation, etc., and all temperature runs for a given composition were on a single sample. All results are reported on a talc-free basis.

The molecular weight of the materials was analyzed by GPC, using polystyrene standards in chloroform at 35°C, with a refractive index detector. Molecular weights are reported in the appropriate tables.

Data for Figure 6 came from an assortment of pilot plant samples (number-average molecular weights ranging from 50,000 to 130,000) and from vial polymerizations using known ratios of L-lactide and *meso*-lactide. The pilot plant samples were analyzed by optical rotation (concentration 5 gms/100 mL chloroform) to determine the concentration of *meso*-lactide which had been present in the reaction mixture. Separate optical rotation and gas chromatography analysis of the monomer mixture confirmed that L-lactide and *meso*-lactide are the predominate components when *meso*-lactide is present at a concentration of 20% or less, and only a small correction is required for D-lactide. The samples for Figure 6 were subjected to an annealing procedure to develop crystallinity. The samples were placed in an oven at 105°C for 90 min, then the temperature was lowered 10°C each 30 min, until the temperature reached 45°C.

ANALYSIS

Figure 1 presents the crystallization behavior of polylactide prepared from a monomer mixture containing 3% *meso*-lactide. The data follow the characteristic S-shaped curves of the Avrami profile,[15] shown by the solid curves.

The Avrami equation,

$$x = 1 - e^{-kt^n} \tag{1}$$

where $x = \Delta H_f(t)/\Delta H_f(\infty)$ is the fractional extent of crystallization, was used with a nonlinear least-squares regression package to determine the exponent n, the rate constant k, and the ultimate extent of crystallization, $\Delta H_f(\infty)$, for each DSC run. This method was found to give more consistent values than the traditional linear form:

$$z = \ln[-\ln(1 - x)] = \ln(k) + n \times \ln(t) \tag{2}$$

The linear form requires prior knowledge of $\Delta H_f(\infty)$, which was not available for all runs. Also, the linear form is sensitive to error at both low and high extent of crystallization, as the following analysis demonstrates. The formula for propagation of error gives the error in z as $\varepsilon_z = dz/dx^*\varepsilon_x$. The derivative of the left side of eq. (2) with respect to x is given by

$$\frac{dz}{dx} = \frac{d\{\ln[-\ln(1 - x)]\}}{dx}$$

$$= \frac{-1}{[(1 - x)\ln(1 - x)]} \tag{3}$$

The error, ε_x, is approximately constant at small conversion and $dz/dx \rightarrow 1/x$. The error in z is then given by $\varepsilon_z = c^*1/x$, which goes to infinity for $x \rightarrow 0$.

At large fractional conversions, the error in x is approximately proportional to x, and

$$\varepsilon_z \propto x\frac{dz}{dx} = \frac{-x}{[(1 - x)\ln(1 - x)]} \tag{4}$$

which goes to infinity as $x \rightarrow 1$.

This demonstrates that the linearized form violates the linear regression assumption of constant variance in the error. It should, therefore, be applied only in intermediate ranges of x. Physically, this simply says that the flat portions of the S-shaped curves are not useful regions for obtaining kinetic data. It is also inappropriate to use any form of the

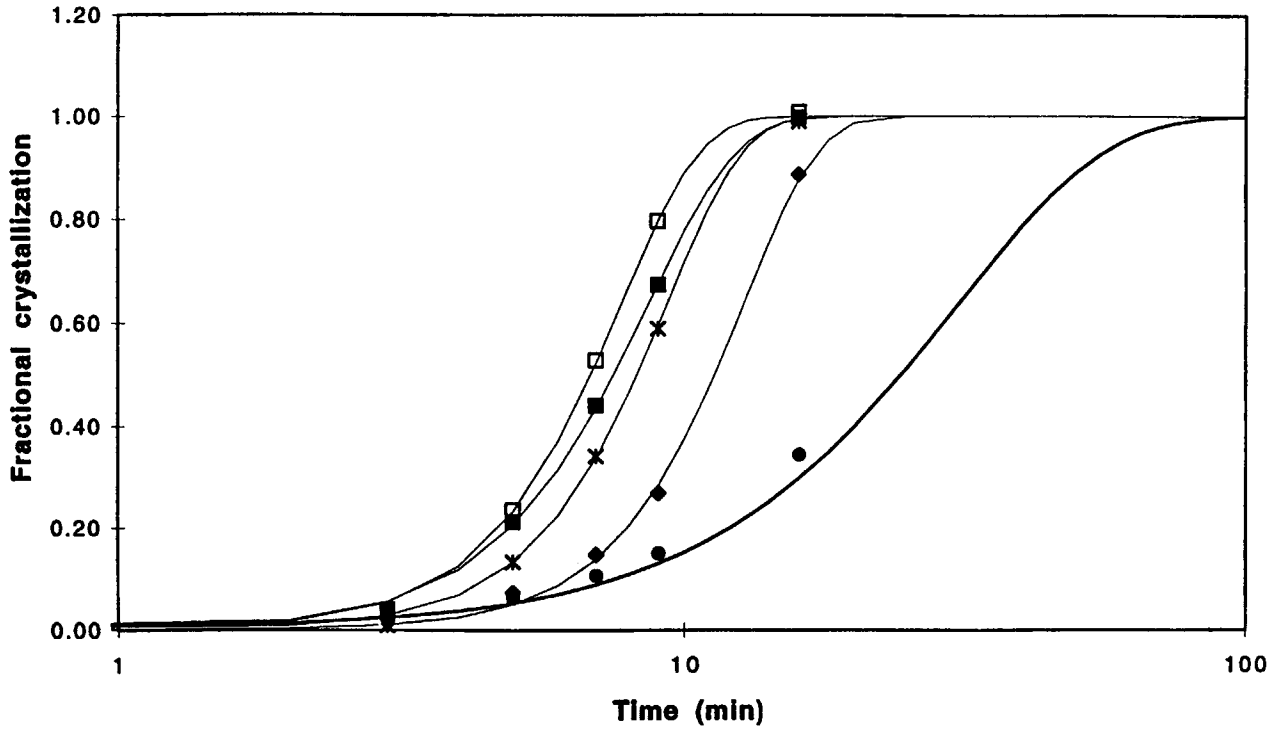

Figure 1 Avrami plots of fractional extent of crystallization. (●) 85°C; (■) 95°C; (✳) 105°C; (□) 115°C; (♦) 125°C.

Avrami equation at high conversion because of the presence of secondary crystallization, which violates the approximations on which the development is based.[15,16]

In a typical Avrami analysis, the rate constant k and the exponent n are estimated from fitting the data using a "measured" value of $\Delta H_f(\infty)$. However, $\Delta H_f(\infty)$ is not always readily available, either because of not crystallizing for a sufficient time or because of secondary crystallization which increases the apparent $\Delta H_f(\infty)$ beyond the value consistent with the Avrami assumptions. The value of the exponent is highly dependent on the value chosen for the ultimate crystallinity. In this analysis, the ultimate crystallinity was regressed simultaneously with the other parameters using nonlinear regression. The $\Delta H_f(\infty)$ values were reasonably constant across the runs at different temperatures. In a few cases (at temperature extremes) the extent of crystallization was not sufficient to reliably determine the ultimate extent, and in those cases the ultimate extent of crystallization from the next higher or lower temperature was used. For the samples made from 6% *meso*-lactide, the 15-min samples were not sufficiently crystallized to determine the ultimate extent of crystallization and the value was measured after annealing as described earlier.

The exponent can be used to obtain information about the nature of the crystallization. This procedure is useful, but does not allow direct comparison of rate constants, because each rate constant has a different dimensionality, depending on the exponent n. To compare rates, the data must either be refit to a single value of n which applies to the entire data set, or another measure of crystallization, such as the crystallization half-time or time to a particular degree of crystallization, must be used. In this paper, the crystallization half-time was determined by fitting each set of data to an Avrami profile and then using the fitted parameters to interpolate or extrapolate to find the time corresponding to $x = 0.5$. The half-times were then used with a uniform value of n to obtain rate constants which had a common dimensionality for model building. The data, as shown below, support the use of a uniform value for n throughout these experiments.

RESULTS AND DISCUSSION

The results will be presented in three sections, covering the effect of meso with no added nucleating agent, the effect of talc as a nucleating agent, and the effect of *meso* for talc-filled samples. A model will then be presented which describes the observed behavior.

Effect of *meso* Level, No Added Nucleating Agent

Tables I and II present the raw crystallization data and the fitted values of $\Delta H_f(\infty)$ and Avrami n for two independent data sets which used varied levels of *meso*. The data were obtained using 15-min isothermal DSC runs. Useful data could be obtained in this way for temperatures from 85°C to 135°C and 0% meso to 6% meso polymer.

The Avrami exponent for these experiments had an average and standard error of 2.8 ± 0.4, with no systematic trend across meso level or across temperature. The measured values of the exponent are consistent with spherulitic growth from nuclei initiated at time zero or with platelike growth from nuclei initiated over time. Spherulitic growth has often been observed in the crystallization of poly(L-lactide)[3-5,17,18] and is believed to be occurring in the present study.

Table III presents the crystallization half-times derived from the raw crystallization data. Both data sets are reported, and although there is some offset in overall rate, the optimal crystallization temperature (105–115°C) is the same for all compositions. The difference between the two data sets is believed to be due to molecular weight, with the higher-molecular-weight samples showing slower crystallization kinetics. The increase in crystallization half-time with increasing meso content is very pronounced. Note that the crystallization half-time for pure poly(L-lactide) agrees with that reported by von Oepen and Michaeli[19] who showed an optimal crystallization temperature of 95–105°C and a half-time of about 2.5 min.

Figure 2 shows the crystallization half-time as a function of meso level for several temperatures and for both sets of data. The plot of $\ln(t_{0.5})$ versus *meso* level gives a reasonably straight line and a consistent slope throughout the region near the optimal crystallization temperature. The slope is approximately 0.37, indicating that the crystallization half-time increases by about 45% for each 1 wt % increase in meso. A model describing this behavior is presented later.

Experiments were also performed on samples polymerized with 9% *meso*-lactide, but less than 1 J/g of crystallinity was observed after 15 min at any of the temperatures of the study. This is understandable based on extrapolation of the data above. At 110°C the estimated $t_{1/2}$ for a polymer from 9% *meso*-lactide is about 60 min. Using $n = 3$ and sub-

stituting in the Avrami equation, it is estimated that at $t = 15$ min the sample would have an extent of crystallization of only $x = 0.01$, corresponding to only about 0.3 J/g and consistent with these observations.

Effect of Talc as a Nucleating Agent

The crystallization half-times for poly(lactide), even for pure poly(L-lactide), are slow compared to the cycle times typical of injection molding processes. For commercial utility it is necessary to reduce the crystallization half-time. A variety of nucleating agents were tested for their ability to enhance the rate of crystallization from the melt. Talc was found to be one of the more effective agents.

Table IV presents the results of adding various levels of talc to a polymer made from 91% L-lactide and 9% *meso*-lactide. Each of these talc-filled samples developed measurable crystallinity, in contrast to the results for the 9% *meso* copolymer without talc, which showed no measurable crystallinity after 15 min. The Avrami exponents for these experiments showed no trend with talc level and averaged 2.6 ± 0.5 at 90°C, which is not significantly different from the value of 2.8 ± 0.4 determined for the talc-free samples. The data at 105°C were too scattered to obtain meaningful values. Rate constants were calculated from the half-times in order to quantify the effect of talc. Figure 3 shows the calculated rate constant based on the half-times and an Avrami exponent of 3. The figure clearly shows that, at 90°C, increasing levels of talc continue to increase the crystallization rate constant over the range from 2% talc to 21% talc. At 105°C the effect levels off after 11% talc.

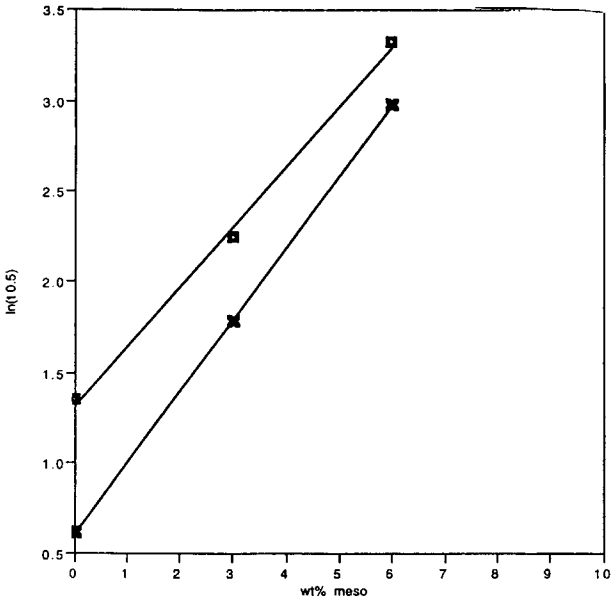

Figure 2 Dependence of crystallization half-time on optical composition, nonfilled samples: (□) 100°C; (×) 110°C.

The rate constant for 0% talc can be estimated from the intercept of the plot. Unfortunately, the relative standard error of the estimate from these data is large and only a rough estimate is possible. However, it provides a useful consistency check with the talc-free data presented earlier. The highest value of the intercept was at 90°C, with an estimated value of 1.5×10^{-5} min^{-3}. Based on that rate constant, the expected crystallinity for a 15-min isothermal run is only 1.5 J/g, which is reasonably consistent with the experimental observation of less than about 1 J/g detected at any temperature of this study. The rate constant corresponds to a

Table III Crystallization Half-times (min)

Temperature (°C)	0% *meso*		3% *meso*		6% *meso*	
	M_n = 101 K	M_n = 157 K	M_n = 88 K	M_n = 114 K	M_n = 58 K	M_n = 114 K
85	14.8		23.9			
90	7.0	11.4	11.0			
95	4.5		8.1			
100	3.8	4.8	9.4	11.4	27.8	
105	2.9		8.6		19.6	
110	1.9	4.0	6.0	10.8	19.7	44
115	3.5		6.9		22.2	
120	4.0	5.7	8.2	11.6		
125	5.1		11.5			
130	8.7	13.4				
135	22.9					

half-time of greater than 35 min for a 9% *meso* sample, consistent with the earlier estimate of roughly 60 min.

Effect of *meso* Level, Talc-filled Samples

A series of isothermal tests at short holding times were made at a talc level of 6 wt % for various meso levels and temperatures. The nature of these tests did not allow determination of Avrami n values, but the crystallization half-times are shown in Table V. As seen in the table, the 0% meso, 6% talc-filled sample crystallized too fast to allow determination of the crystallization half-time (the limit of the DSC is approximately 1 min, as that is the settling time after quenching the melt). The 3% meso, 6% talc-filled sample was also too fast to measure at the optimal crystallization temperature of 110°C.

Figure 4 presents the results on talc-filled samples as a function of *meso* level at various temperatures. As with Figure 2, for nonfilled samples, the $\ln(t_{0.5})$ versus weight percent meso is approximately linear. The slope for talc-filled samples is 0.27. This indicates that the crystallization half-time (in the region of optimal temperature) increases by about 31% for each 1 wt % increase in meso content. The model developed below explains this effect based on the entropic contribution to the free energy of crystallization, expressed primarily through the melting point depression for the copolymers.

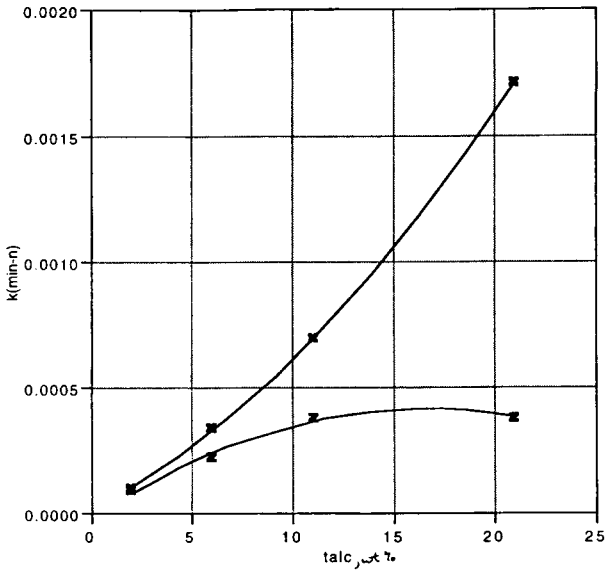

Figure 3 Dependence of crystallization rate constant on talc content, 9 wt % *meso*-lactide in monomer mixture, (×) 90°C; (Z) 105°C.

MODEL

The rate of crystallization as a function of temperature, optical composition, and nucleating agent can best be described by decomposing the overall Avrami rate constant into component parts. The overall rate of crystallization is dependent on the concentration of growing spherulites and the rate of spherulite growth. For instantaneous nucleation with spherulitic growth (Avrami $n = 3$), the rate constant[15] is given by

$$k = \tfrac{4}{3}\pi NG^3 \qquad (5)$$

where N is the density of primary nucleation sites to initiate spherulitic growth and G is the lineal

Table IV Isothermal Crystallization Results for Talc-filled Samples of Poly(91% L-lactide-*co*-9% *meso*-lactide)

Sample	3 min	6 min	9 min	13 min	16 min	$H_f(\infty)$	n	Half-time (min)
90°C								
2 wt % talc	0.5	1.4	2.3	5.9	10.0	(29.5)	2.7	18.9
6 wt % talc	1.3	4.0	7.6	15.1	21.2	(29.5)	2.3	12.7
11 wt % talc	1.0	2.8	11.3	23.0	28.2	29.5	3.3	10.0
21 wt % talc	2.0	10.7	18.5	24.3	26.2	26.3	2.2	7.4
105°C								
2 wt % talc	0	0	0.3	0.7	6.4	—	—	19.6
6 wt % talc	0.4	0.5	0.9	2.5	19.7	—	—	14.6
11 wt % talc	0.9	1.3	4.8	—	26.6	—	—	12.2
21 wt % talc	0.3	0.6	1.1	4.2	28.2	—	—	12.2

Enthalpy in J/g, PLA basis. $H_f(\infty)$ values in parentheses are from adjacent temperature, rather than determined from nonlinear fit. Data at 105°C not sufficient for determination of $H_f(\infty)$ and n. Number-average molecular weights: 39 K for 2% talc, 46 K for 6% talc, 55 K for 11% talc, and 53 K for 21% talc.

growth rate of a spherulite. The density of primary nucleation sites, N, is expected to depend on the history of the polymer (because of residual crystallites and other heterogeneities) and on the concentration of nucleating agent. The lineal growth rate of a spherulite, G, is expected to depend on the polymer properties and temperature.

Solid nucleating agents, such as talc, have been shown to increase N but to make no change in G for crystallization of poly(ethylene terephthalate) (PET).[20] This is consistent with the expectation that a solid nucleating agent acts to change the number of primary nucleation sites, N, but does not affect the secondary nucleation processes which determine G. For this work, it has been shown that the presence of talc, at levels up to 11 wt %, resulted in an almost linear increase in the measured Avrami rate constant. The nucleation density term, N, can therefore be represented as

$$N \propto 1 + B^{*}\text{wt \% talc} \qquad (6)$$

where B is an appropriate conversion factor. In the development which follows it has been assumed that the number of nucleation sites is independent of optical composition, and that the dependence of rate on optical composition is determined by the spherulite growth rate, G. The proportionality factor for eq. (6) cannot be determined without an independent measurement of either N or G. Hot-stage optical microscopy is one method which can be used to separate these two factors[3,20] and to check the assumption that N is independent of optical composition.

Hoffman and colleagues[21] give an excellent description of polymer crystallization at the lamellar level and derive a theoretical expression for the growth rate, G, of a homopolymer

$$G = G_0 e^{-U^{*}/R(T-T_\infty)} e^{-K_g' T_m / T\Delta T f} \qquad (7)$$

where $K_g' = K_g / T_m = \dfrac{2b\sigma\sigma_E}{k\Delta H_f}$.

This expression for the growth rate, G, consists of three factors. First, a preexponential factor, G_0, which includes molecular weight effects. The second factor is a transport term for local motion, and the third factor describes the rate of nucleation for lamellar growth (secondary nucleation). Vasanthakumari and Pennings[3] have measured G for poly(L-lactide) as a function of molecular weight and temperature and demonstrated that below 163°C the growth was spherical and in regime II, with K_g as given above.

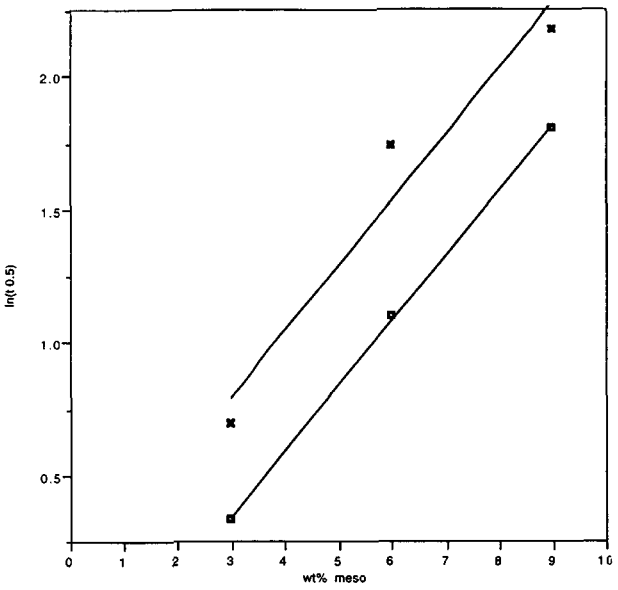

Figure 4 Dependence of crystallization half-time on optical composition, talc filled samples, (×) 90°C; (□) 100°C.

The dependence of G_0 on molecular weight is not well defined. Van Antwerpen and van Krevelen[20] reported G_0 for seven PET samples of varying molecular weight, showing a linear dependence of G_0 on $1/M_n$. However, when extrapolated to molecular weights above 60,000 the correlation failed, giving physically unrealizable negative values. Refitting their data to the inverse molecular weight, squared, gave nearly as good correlation and maintained positive G_0 for all values of M_n. Vasanthakumari and coworkers[3,5] reported G_0 for four samples of PLA, with varying molecular weight. A fit of their data to

Table V Crystallization Half-times (min) for Polylactide Samples with 6 wt % Talc

Temperature (°C)	0 wt % *meso* (M_n = 123 K)	3 wt % *meso* (M_n = 105 K)	6 wt % *meso* (M_n = 122 K)	9 wt % *meso* (M_n = 81 K)
90	< 1	2.0	5.7	8.8
100	< 1	1.4	3.0	6.0
110	< 1	< 1	3.9	10.0
120	< 1	2.1	14.7	⩾ 15

inverse molecular weight squared was also reasonably linear, and such a dependence was chosen for the model developed here. A linear model was also tested on the current data set, but a satisfactory fit could not be obtained.

For poly(L-lactide) homopolymer, the remaining terms have been evaluated. Vasanthakumari and colleagues[3,5] obtained a very good fit to their data with the following parameter values (independent of temperature or molecular weight):

U^*	activation energy for local motion (1500 cal/mol)
R	gas constant (1.987 cal/mol)
T	crystallization temperature
T_∞	temperature at which flow ceases (T_g − 30°C = 300 K)
K_g	nucleation parameter for lamellar growth
ΔT	undercooling ($T_m - T$)
f	factor to account for change in heat of fusion with temperature [$2T/(T_m + T)$]
T_m	equilibrium melting temperature (480 K)
b	surface nucleus thickness ($5.2*10^{-10}$ m)
σ	lateral surface energy
σ_e	fold surface free energy ($\sigma\sigma_e = 733*10^{-6}$ J^2/m^4)
ΔH_f	heat of fusion ($111*10^{+6}$ J/m^3)
k	Boltzmann constant ($1.38*10^{-23}$ J/K)

A number of new considerations must be made for crystallization of copolymers. First, as discussed by Mandelkern,[16] is the effect that the composition is changing as the crystallization proceeds, resulting in a drop in T_m. This effect can cause a deviation from Avrami behavior at low undercoolings. In the present work, the undercooling is high (≅100°C) and this effect can be neglected. Also, the low meso levels and low overall extent of crystallization for PLA make the concentration effect less important.

Second, there may be a decrease in the rate of primary nucleation. Mandelkern derives an expression quantifying this relationship for homogeneous nucleation. This factor is believed to be unimportant in the present system because the nucleation is behaving as instantaneous, heterogeneous nucleation.

Third, there is a decrease in equilibrium melting point. There are at least two possible explanations for this effect. In one treatment[22] it is assumed that the noncrystallizable units are incorporated into the crystal structure as defects. This results in a decrease in the equilibrium melting point, T_m, because of the decrease in the enthalpy of fusion. In the other extreme, it is assumed that the noncrystallizable units are rejected from the crystal structure.[23] This retains the same enthalpy of fusion but cause a reduction in T_m because of the entropy effect of separating the two types of monomer units. As shown by Sanchez and Eby,[22] the models cannot be distinguished on the basis of melting point behavior. The melting point change will be explicitly considered in this model.

Finally, an entropic contribution for selecting crystalline sequences needs to be included in the expression for secondary nucleation.[16,24] The expression for a copolymer with volume fraction ϕ_2 of crystallizable units is

$$G = \phi_2 G_0 e^{-U^*(\phi)/R[T-T_\infty(\phi)]} e^{-K_g' T_m(\phi)/T\Delta T(\phi) f(\phi)} \times e^{2\sigma T_m(\phi)\ln(\phi_2)/bf(\phi)\Delta H_f \Delta T(\phi)} \quad (8)$$

where the new exponential term is the entropic contribution for selecting crystalline sequences.

Polylactide copolymers are an interesting special case of copolymers because only the stereochemistry, not the overall composition, is changed. Optical isomers have many properties which are identical, so the effect of composition will show up in fewer terms than for some other copolymers. In particular, G_0 is not expected to depend on optical composition. The transport factor, U^*, is also expected to have no significant dependence on optical composition. The glass transition temperature, T_g, changes relatively little across the entire range from poly(L-lactide) to poly(*meso*-lactide), so $T - T_\infty$ is also essentially independent of composition in the range studied here.

The nucleation rate term and entropic sequencing term include many individual parameters, each of which is expected to be nearly independent of optical composition. In particular, the surface free energies, σ and σ_e, are related to the energy required to bend a chain back onto itself and are not expected to be affected by optical composition. This has been observed in various polymer blends[25-27] although it was not found to be the case when the two polymers of a blend had greatly different conformational characteristics.[28]

The enthalpy of fusion, per unit volume of crystallite, is also taken as constant, consistent with the Flory theory. The data of Fischer and coworkers[8] show significant incorporation of D-units into the crystal structure of poly(L-lactide-*co*-D-lactide) at low undercoolings but at high undercooling the D-units are rejected. The undercoolings in this study are very high and for this discussion it will be considered that the D-units are rejected, following the theory of Flory. Thus, ΔH_f is expected to be independent of composition.

The final factor, the surface nucleus thickness, b, is independent of composition under this same hypothesis.

The expression for G, the spherulite growth rate, then depends on optical composition only through the direct composition terms [ϕ_2 and $\ln(\phi_2)$] and through the effect of composition of the equilibrium melting point terms. It is difficult to experimentally determine the equilibrium melting point for copolymers because of the broad melting-point range.[16,23] The melting-point depression as a function of composition, $T_m - T_m(\phi)$, is derived from Flory's equation for random copolymers:

$$\frac{1}{T_m(\phi)} = \frac{1}{T_m} - \frac{R}{\Delta H_f} \ln(1 - p_1) \tag{9}$$

or

$$T_m - T_m(\phi) = \frac{-RT_m(\phi)T_m}{\Delta H_f} \ln(1 - p_1) \cong \frac{RT_m^2 p_1}{\Delta H_f} = \gamma\phi_1 \tag{10}$$

where $\gamma = RT_m^2/\Delta H_f$ and p_1 is the probability that the next residue in a crystallizing chain will be a defect. The values of ΔH_f and ϕ must be chosen on a self-consistent basis. For convenience, here we will say that M_n = 144, ΔH_f = 3.2 kcal/mol, and ϕ_1 is the *meso*-lactide mole fraction. A linear dependence of melting-point depression on volume fraction is also obtained for the crystal defect model of Sanchez and Eby.[22] For now, γ will be treated as an adjustable parameter.

With this expression [eq. (10)] for the melting-point depression, eq. (8) can be rewritten to show the dependence of crystallization rate on optical composition.

$$\frac{G(\phi)}{G(100\%L)} = \phi_2 e^{(K_g'/2T^2)\{[T_m(T_m+T)/(T_m-T)] - [(T_m-\gamma\phi_1)(T_m+T-\gamma\phi_1)]/(T_m-T-\gamma\phi_1)\}} \times e^{(2\sigma/b\Delta H_f)\{[\ln(\phi 2)(T_m-\gamma\phi_1)(T_m+T-\gamma\phi_1)]/[2T(T_m-T-\gamma\phi_1)]\}} \tag{11}$$

Letting $S = \dfrac{kT_m}{b^2\sigma_E}$, approximating $\ln(\phi_2) = \ln(1 - \phi_1) \cong -\phi_1$, expanding and collecting terms gives, for the exponential power terms,

$$\frac{K_g'}{2T^2\Delta T(\Delta T - \gamma\phi_1)} \times \left\{ \begin{aligned} &\phi_1[-2\gamma T^2 + \gamma(\Delta T)^2 - ST(T_m^2 - T^2)] \\ &+ \phi_1^2[-\gamma^2\Delta T - S\frac{T}{T_m}\gamma(T^2 + TT_m - 2T_m^2)] \\ &+ \phi_1^3\left(-\gamma S \frac{T}{T_m}\Delta T\right) \end{aligned} \right\} \tag{12}$$

For $\phi_1 \leq 0.1$ and for reasonable values of the other parameters, direct substitution shows the terms in ϕ_1^2 and ϕ_1^3 to be small compared to the ϕ_1 term. It is also readily seen that $\gamma(\Delta T)^2 \ll 2\gamma T^2$, so the function can be approximated as

$$\frac{-K_g'\phi_1}{\Delta T(\Delta T - \gamma\phi_1)}\left\{\gamma + \frac{S}{2}T\left[\left(\frac{T_m}{T}\right)^2 - 1\right]\right\} \tag{13}$$

The data were fit to this model and to a simplified model retaining only the first term in brackets. It was found that the simplified model was adequate for fitting the data, with little reduction in error using the more complete model. The simplified model,

$$G(\phi) = G(100\%L)\phi_2 e^{-K_g'\gamma\phi_1/\Delta T(\Delta T-\gamma\phi_1)} \cong G(100\%L)e^{-K_g'\gamma\phi_1/\Delta T(\Delta T-\gamma\phi_1)} \tag{14}$$

shows how the lineal growth rate varies as a function of composition. Combining eqs. (5), (6), (7), and (14), with the inverse molecular weight squared dependence for G_0, gives the final model for the Avrami rate constant:

$$\ln(k) = A + \ln(1 + B^*\text{wt \% talc}) + 3\ln\left[1 + \left(\frac{C}{M_n}\right)^2\right] - \frac{3U^*}{R(T - T_m)} - \frac{3K_g}{T(T_m - T)f} - \frac{3\dfrac{K_g}{T_m}\gamma\phi_1}{(T_m - T)(T_m - T - \gamma\phi_1)} \tag{15}$$

The parameters of this model were separately fit to the data of Table V (6% talc) and Table III (no talc) using nonlinear regression. The two data sets gave very similar results for γ, U^*/R, and K_g, showing each of these parameters to be independent of the presence of a primary nucleating agent. The data

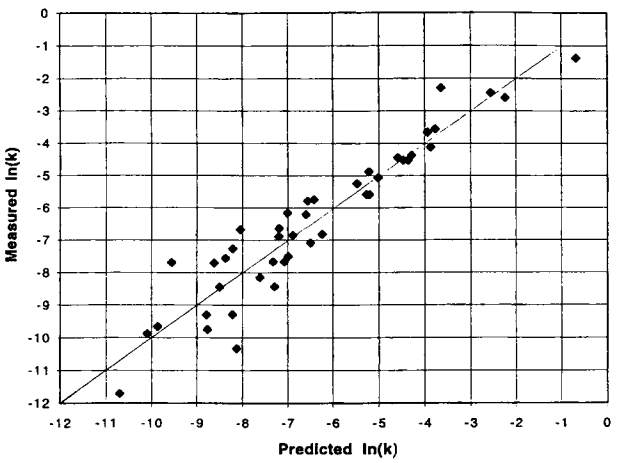

Figure 5 Measured versus predicted rate constants.

sets were combined and the final parameters were determined:

Parameter value (estimated standard error)
A = 68.0 (7.3)
B = 84.5 (wt %)$^{-1}$ (37)
C = 76900 (18800)
U^*/R = 675 K (64)
K_g = 535000 K^2 (54000)
γ = 267 K (22)

Figure 5 shows predicted versus measured rate constants for the samples in this study. The agreement over a wide range of rates is satisfactory and this model can be used to predict crystallization rates for a range of optical composition, talc levels, and temperatures. The molecular weight dependence has been accounted for in a preliminary manner, based on limited data. It is anticipated that the model will also hold for random copolymers of poly(L-lactide-*co*-D-lactide), with $\phi_1 = x_D$.

MODEL CROSSCHECKS

The relationship between U^*/R and K_g determines the maximum crystallization temperature. They are highly correlated, and the limited temperature range leads to high uncertainties in their values. The value for U^*/R is similar to the value of 750 K reported to hold for many polymers by Hoffman and coworkers[21] and used by Vasanthakumari and Pennings.[3] The value of K_g is considerably higher than that reported by Vasanthakumari. The maximum crystallization rate for Vasathakumari was at 130°C, whereas in this study and that of von Oepen and Michaeli[19] the maximum was found at about 110°C. The method of determination was different (optical versus DSC), but the maximum in G and k are expected to occur at the same temperature[16] when heterogenous nucleation predominates. The current data sets gave parameters which correspond to a maximum rate for poly(L-lactide) at 109°C with only a slight dependence on meso level. The maximum rate for 6% meso is calculated to be at 102°C.

The value for γ, 267 K, is somewhat higher than the theoretical value of 143 K calculated from eq. (10). The regressed value of γ is, however, reasonably close to the measured value based on the reduction in peak melting point. Figure 6 shows experimental data on peak melting temperature versus optical composition for a number of poly(L-lactide-*co*-*meso*-lactide) samples which were annealed at temperatures of about 90 to 110°C. The figure shows a reduction in melting point of about 30 K for every 10% meso, corresponding to a value for γ of 300 K. These results show that the model provides a better fit to the data when γ is taken to represent the apparent, nonequilibrium, melting-point reduction for the copolymers rather than the theoretical limiting value.

The increase in nucleation density for addition of talc is readily calculated from eq. (6). Combining and solving for the nucleation density ratio gives

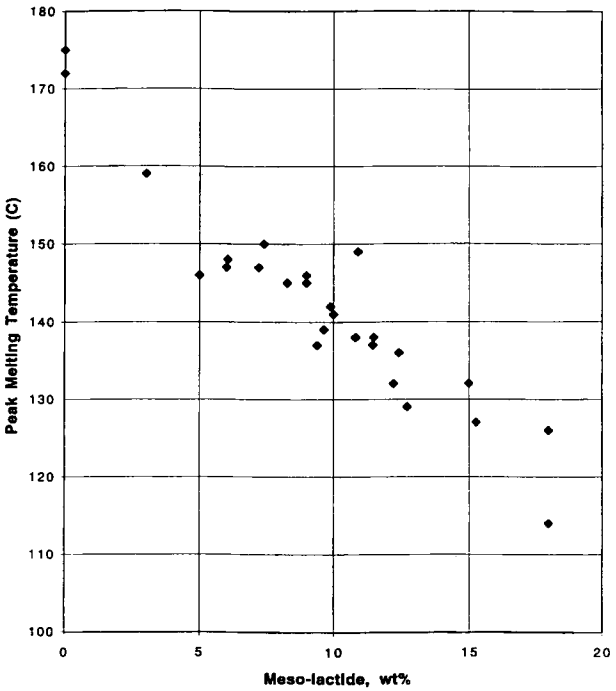

Figure 6 Peak melting temperature versus optical composition.

$$\frac{N(\text{talc})}{N(\text{blank})} = 1 + B \times \text{wt \% talc} \qquad (16)$$

For 6 wt % talc this gives a nucleation density ratio over 500. From eqs. (1) and (5), it follows that for spherulitic growth the crystallization half-time is proportional to nucleation density, N, to the one-third power. The increase in nucleation density is sufficient to reduce the crystallization half-time for pure poly(L-lactide) from 3 min at 110°C for the base case to approximately 25 s at 110°C with 6 wt % talc added. For a sample with 3% mesolactide copolymerized with the L-lactide, the half-time goes from about 7 min, base case, to about 1 min for 6 wt % talc added. For these low *meso* levels this may be sufficient to allow crystallization in commercial injection-molding processes. Higher talc levels or more effective nucleating agents would be useful, especially for samples with higher *meso* content.

As a final validation, the relationship between crystallization half-time and *meso* level will be explored. Equation (1) and the definition of half-time gives, for $n = 3$,

$$\ln(t_{0.5}) = -\tfrac{1}{3}\ln[\ln(0.5)] - \tfrac{1}{3}\ln(k) \qquad (17)$$

From eq. (15), at any given temperature, molecular weight, and talc level, a plot of $\ln(t_{0.5})$ versus ϕ_1 will be approximately linear, with a slope of

$$\ln(t_{0.5}) \propto \frac{\frac{K_g}{T_m}\gamma}{(T_m - T)(T_m - T - \gamma\phi_1)} \qquad (18)$$

For large undercooling and small ϕ_1 this gives $\ln(t_{0.5})$ proportional to *meso* content, with a slope of approximately

$$\frac{\frac{K_g}{T_m}\gamma}{(T_m - T)^2} \times \frac{1}{100} \qquad (19)$$

where the 1/100 factor converts from wt % *meso* to ϕ_1.

This is consistent with the linear behavior observed in Figures 2 and 4, with calculated slopes of 0.21 at 90°C, 0.26 at 100°C, and 0.31 at 110°C, in good agreement with the observed slope of 0.34 for all data sets combined.

CONCLUSIONS

The crystallization kinetics of poly(L-lactide-*co*-*meso*-lactide) are strongly dependent on the copolymer composition. The crystallization half-time increases by roughly 40% for every 1 wt % increase in the mesolactide content of the polymerization mixture. This strong dependence on optical purity presents an opportunity to control polymer properties through optical composition, while mandating good manufacturing processes in order to maintain high optical purity throughout the lactic acid, lactide, and polylactide production processes. The dependence of the crystallization kinetics on the optical purity is adequately described using the Hoffman–Lauritzen kinetic equation, modified for copolymers.

The optical copolymers of polylactide present a special case for copolymers, because only the configuration changes, with minimal changes in T_g, melt viscosity, or other properties which might affect crystallization kinetics. The ring-opening polymerization of optically active monomers affords a very convenient and easily manipulated model system for crystallization studies.

Nonlinear fitting of the raw crystallization data to the untransformed Avrami equation led to consistent estimates of crystallization rate constants, which were then used in the Hoffman–Lauritzen formulation to measure the effect of talc and optical purity. The parameters needed to fit the data are the correct order of magnitude based on theory, and demonstrate that the decrease in crystallization rate for this system is dominated by the reduction in melting point.

The model, reduced to simplest form, predicts that the log of the crystallization half-time should be a linear function of optical purity. This agrees with the experimental observations.

Talc was found to perform as a nucleating agent, with 6 wt % talc giving a 500-fold increase in the nucleation density.

The experimental portion of this work was performed by Nancy Buehler and Greg Schmidt; their contributions and careful work are greatly appreciated. Thank you to all of my colleagues at Cargill for their support and to Cargill, Inc. for funding the work. This work was partially funded through ATP agreement #70NANB5H1059.

REFERENCES

1. P. R. Gruber, E. S. Hall, J. J. Kolstad, M. L. Iwen, R. D. Benson, and R. L. Borchardt, U.S. Pat. 5,142,023 (1992).

2. A. J. Nijenhuis, D. W. Grijpma, and A. J. Pennings, *Polym. Bull.*, **26,** 71 (1991).
3. R. Vasanthakumari and A. J. Pennings, *Polymer,* **24,** 175 (1983).
4. B. Kalb and A. J. Pennings, *Polymer,* **21,** 607 (1980).
5. K. Kishore and R. Vasanthakumari, *J. Polym. Sci.,* **22,** 537 (1984).
6. D. Cohn, H. Younes, and G. Marom, *Polymer,* **28,** 2018 (1987).
7. C. Migliaresi, A. DeLollis, L. Fambri, and D. Cohn, *Clin. Mat.,* **8,** 111 (1991).
8. E. W. Fischer, H. J. Sterzel, and G. Wegner, *Kolloid-Z.u.Z. Polymere,* **251,** 980 (1973).
9. G. L. Loomis and J. R. Murdoch, U.S. Patent 4,902,515, 1990.
10. M. Spinu, U.S. Patent 5,317,064, 1994.
11. H. Tsuji and Y. Ikada, *Macromolecules,* **26,** 6918 (1993).
12. Y. Ikada, K. Jamshidi, H. Tsuji, and S. H. Hyon, *Macromolecules,* **20,** 904 (1987).
13. D. D. Deane and E. G. Hammond, *J. Dairy Sci.,* **43,** 1421 (1960).
14. M. Muller, J. Hess, W. G. Schnell, D. Bendix, and G. Entenmann, U.S. Patent 4,983,745, 1991.
15. M. Avrami, *J. Chem. Phys.,* **8,** 212 (1940).
16. L. Mandelkern, *Crystallization of Polymers,* McGraw-Hill, New York, 1964.
17. B. K. Carter and G. L. Wilkes, *Polym. Prepr.,* **24,** 77 (1983).
18. B. K. Carter and G. L. Wilkes, *Polym. Prepr.,* **24,** 90 (1983).
19. R. von Oepen and W. Michaeli, *Clin. Mat.,* **10,** 21 (1992).
20. F. van Antwerpen and D. W. van Krevelen, *J. Polym. Sci.,* **10,** 2423 (1972).
21. J. D. Hoffman, G. T. Davis, and J. I. Lauritzen, in *Treatise on Solid State Chemistry,* Vol. 3, N. B. Hannay, Ed., Plenum Press, New York, 1976.
22. I. C. Sanchez and R. K. Eby, *J. Res. Natl. Bur. Stand. -A,* **77,** 353 (1973).
23. P. J. Flory, *Trans. Faraday Soc.,* **51,** 848 (1955).
24. J. Boon and J. M. Azcue, *J. Polym. Sci., Part A-2,* **6,** 885 (1968).
25. G. C. Alfonso, V. Chiappa, J. Liu, and E. R. Sadiku, *Eur. Polym. J.,* **27,** 795 (1991).
26. T. T. Wang and T. Nishi, *Macromolecules,* **10,** 421 (1977).
27. B. S. Hsiao and B. B. Sauer, *J. Polym. Sci., Polym. Phys. Ed.,* **31,** 901 (1993).
28. B. De Carvalho and R. E. S. Bretas, *J. Appl. Polym. Sci.,* **55,** 233 (1995).

Received October 23, 1995
Accepted March 18, 1996